

THEORETICAL ANALYSIS AND EXPERIMENTAL  
VERIFICATION OF A MONOPROPELLANT DRIVEN  
FREE PISTON HYDRAULIC PUMP

By

Timothy Garland McGee

BS University of Illinois at Urbana-Champaign 2001

A report submitted in partial satisfaction of the  
Requirements for the degree of

Masters of Science, Plan II

in

Mechanical Engineering

at the

University of California at Berkeley

Committee in Charge:

Professor Homayoon Kazerooni, Chairman

Professor Carlos Fernandez-Pello

Spring 2003

## **Abstract**

### **DYNAMIC ANALYSIS AND EXPERIMENTAL TESTING OF A NOVEL MONOPROPELLANT DRIVEN FREE PISTON HYDRAULIC PUMP**

by

Timothy G. McGee

Master of Science in Engineering – Mechanical Engineering

University of California, Berkeley

Professor Hodayoon Kazerooni, Chair

The lack of compact, efficient, and lightweight power sources currently prevents the more widespread use of mobile robotic devices capable of autonomous operation for periods beyond a few minutes. While technology for information processing, communication, and control systems has accelerated, similar breakthroughs for power sources have not kept pace. This report presents a novel free piston hydraulic pump (FPHP) to supply hydraulic power to mobile robotic systems. The basic design incorporates several innovative features. High concentration monopropellant fuel (e.g. hydrogen peroxide) decomposes into high temperature gases when exposed to a solid catalyst bed. The energy released by the reaction can be harnessed in a novel engine/pump that produces high-pressure hydraulic flow to power actuators. Since the reaction does not require an oxidizer, fuel/oxidizer mixing is eliminated. This allows the design of simple, lightweight systems with increased power and energy density, and operation in oxygen free environments, such as underwater and space. The design, unlike the internal combustion engine, produces power on demand, eliminating idling when there is no load on the system. Steam and oxygen, which are nontoxic to humans, are the only byproducts of this power supply, and for many applications it will have no traceable signature. A theoretical thermodynamic analysis has been performed to aid in design of the system, and an experimental monopropellant FPHP has been built and tested. The prototype successfully pumped hydraulic fluid, although the flow rate was limited by the off-the-shelf components used.

## **Acknowledgements**

- Professor Homayoon Kazerooni, the project advisor, provided outstanding support and encouragement to push technological boundaries and explore our novel ideas.
- Justin Raade was an excellent research partner, and it was a pleasure to work with him.
- Mark Ventura and Eric Wernimont at General Kinetics provided outstanding technical assistance to ensure the design of a safe hydrogen peroxide system.
- The research of Professors Michael Goldfarb and Eric Barth at Vanderbilt University on using monopropellant fuels for robotic applications helped inspire our project.
- Ted Getchell, director of the University's Richmond Field Station facilities, supported our efforts to safely bring hydrogen peroxide fuel into our laboratory.
- The Air Force Office of Scientific Research funded my National Defense Science and Engineering Graduate Fellowship, which helped to support my work on this project.
- My parents, Max and Clare McGee, have always been a crucial source of support and guidance throughout all of my endeavors.

## Table of Contents

1.	Introduction	6
2.	Description of Free Piston Hydraulic Pump	9
3.	Hydrogen Peroxide as a Monopropellant	11
4.	Dynamic Analysis of Free Piston Hydraulic Pump	13
4.1.	Theoretical Modeling	13
4.2.	Simulation Results	16
5.	Experimental Free Piston Hydraulic Pump	20
5.1.	Hardware	20
5.2.	Experimental Results	22
6.	Discussion	25
7.	Conclusions	29
8.	References	30
9.	Appendix A. Derivation of Hot Gas Dynamics Equation	31
10.	Appendix B. Safety Procedures for H <sub>2</sub> O <sub>2</sub> System Design and Handling	35
10.1.	Materials and Passivation	35
10.2.	Pressure Relief and Fuel Dump Valve	35
10.3.	Personal Safety Equipment	36
10.4.	Training	36
10.5.	Disposal of H <sub>2</sub> O <sub>2</sub>	36
10.6.	Emergency Situation Procedure	37
11.	Appendix C. Photographs of Experimental System	38

## List of Tables

Table 1. Comparison of Various Hydrogen Peroxide Concentrations .....	12
Table 2. Design Simulation Parameters.....	17

## List of Figures

Figure 1. Monopropellant Powered Free Piston Hydraulic Pump.....	9
Figure 2. Operation of Free Piston Hydraulic Pump .....	10
Figure 3. Free Body Diagram of Free Piston Assembly.....	13
Figure 4. Model of Fuel Flow Through Valve.....	15
Figure 5. Simulation Results for Free Piston Assembly Velocity and Position .....	18
Figure 6. Simulation Results for Hot Gas Pressure .....	19
Figure 7. Photo of the Experimental Power Source.....	20
Figure 8. Schematic of Monopropellant Fuel System .....	21
Figure 9. Hydraulic System for Free Piston Hydraulic Power Source .....	22
Figure 10. Experimental Accumulator Pressure with Manual Fuel Valve Pulse .....	23
Figure 11. Experimental Hot Gas Pressure with 500ms Injection Time .....	24
Figure 12. Experimental Hot Gas Pressure Over Single Stroke .....	24
Figure 13. Photo of Interface Between Fuel Valve and Catalyst.....	26
Figure 14. Diagram of Interface Between Fuel Valve and Catalyst.....	26
Figure 15. Comparison of Experimental Data with Modified Simulation.....	27
Figure A-1. Control Volume for Hot Gas Cylinder.....	32
Figure C-1. Disassembled FPHP .....	38
Figure C-2. Close up of Fuel Valve – Catalyst Bed Assembly .....	38
Figure C-3. Catalyst Bed.....	39
Figure C-4. Safety Testing of System at General Kinetics' Facility .....	39
Figure C-5. Loading Hydrogen Peroxide Propellant .....	40
Figure C-6. Successful Test of FPHP Using Compressed Air.....	40

## 1. Introduction

The limitation of current power sources is one of the dominant bottlenecks preventing the more widespread appearance of fully autonomous field robotics. These robotic systems include any automated mobile platforms such as walking machines, robotic fish, or any similar system that must maintain energetic autonomy in non-laboratory environments. There are many difficult problems associated with field robotics such as design, control algorithm, navigation, sensors, and electronics. All of these problems are difficult but solvable with current technology. However, to overcome the power supply problem in past research efforts, researchers have typically either used a large number of batteries to demonstrate the system performance for a short time in the field, or they used an umbilical cord to power their system from an AC power source or other centrally located hydraulic or pneumatic power supply. Thus, in order to achieve true energetic autonomy for mobile robotics, new advances in power source technology are still required.

Most human scale and smaller robotic systems have power requirements ranging from 10W to 2000W. The dominant traditional power supplies in this range are electric batteries, fuel cells, and small internal combustion (IC) engines, such as model airplane engines. These power supplies have significant drawbacks, however. The low energy density<sup>1</sup> of batteries prevents them from being applicable for any prolonged period of time. Although fuel cells do have larger energy density than batteries, they lack high power density<sup>2</sup> and cannot create bursts of power quickly. Electric actuators are also much larger and bulkier than hydraulic or pneumatic actuators for comparable power outputs. While the high energy density of gasoline is desirable, all hydrocarbon engines require elaborate systems for air compression and ignition in addition to many moving parts such as crankshafts and pistons. Small IC engines must also run at extremely high speeds in order to achieve good power densities. Thus, large, complicated gear reduction systems are required to connect these engines to pumps.

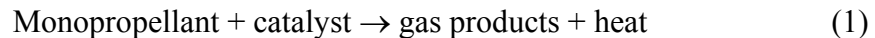
---

<sup>1</sup> Energy density refers to the ratio of the total energy a fueled power supply can deliver over its mass.

<sup>2</sup> Power density refers to the ratio of the power, or rate of energy production, that a power supply can deliver over its mass.

Hydrocarbon engines are also limited by their dependence on the oxygen in air, restricting underwater and space applications.

Given these limitations of more traditional power sources, the use of monopropellant technology for mobile robotic power supplies has promising potential. Monopropellant fuels refer to a class of energetic liquids, such as high concentration hydrogen peroxide and hydrazine, which decompose upon contacting a solid catalyst surface and release heat:



The energy produced by this reaction can be harnessed by allowing the expanding hot gas products to perform work on a piston or turbine, just as the combustion products of an IC engine are used to perform work. Since the monopropellant reaction does not require an oxidizer, fuel/oxidizer mixing is eliminated. This allows the design of simple, lightweight systems with increased power and energy densities, and operation in oxygen free environments, such as underwater or space. Unlike IC engines, monopropellant driven engines do not require a compression stage. This eliminates idling when there is no load on the system, and allows a monopropellant power supply to produce power on demand by producing discrete engine strokes. The ability to control individual strokes of the engine also provides more flexibility for the overall control strategy for the power supply. Furthermore, hydrogen peroxide, one of the available monopropellant fuels, decomposes into steam and oxygen, which are nontoxic to humans and can reduce the signature of the system.

Monopropellants have a successful history of applications. They have most often been used as rocket propellants in spacecraft including the Mercury spacecraft, satellite attitude control, and an experimental Personal Rocket Belt [1]. Monopropellants have also been successfully used to power turbine driven hydraulic pumps for the X-15 Rocket Plane [2] and NASA Space Shuttle [3]. While no literature was found on a detailed study of the use of monopropellants for small scaled robotics applications outside of the recent past, a NASA sponsored technology study from 1967 mentions the possibility of using the hot gas from monopropellant decomposition to power human scaled robotics [4].

More recently, there have been some renewed investigations into the development of monopropellant-fueled power supplies. In his 2001 patent, Amendola outlines the benefits of using various monopropellants, including hydrogen peroxide, to drive a piston engine [5]. Also, a team from Vanderbilt University has recently done some extensive testing using decomposed hydrogen peroxide to directly power hot gas cylinders [6].

The two main approaches for monopropellant robotic power supplies are to use the decomposed hot gases to directly power actuators or to use the decomposed hot gases to power a hydraulic system [4]. Although a monopropellant driven hydraulic system is bulkier and less efficient than a system which directly uses the decomposed hot gases, it does provide several advantages, which could make it more desirable for certain applications. First, since hydraulic fluid is far less compressible than the hot gas, higher bandwidth actuation can be achieved. The higher pressures that can be obtained in hydraulic fluid, when compared to compressed gas, also allow the use of smaller actuators to achieve the same forces. A centralized hydraulic pump also contains the hot decomposition gases to a single location where they can be vented using passive exhaust ports. Thus the need to develop control valves that can withstand the high decomposition temperatures of the monopropellants is eliminated.

This report investigates such a hydraulic system, which uses hydrogen peroxide to drive a novel free piston hydraulic pump (FPHP). The FPHP combines two past areas of research: the use of monopropellants to power hydraulic systems with turbine driven pumps [2,3] and free piston hydraulic pumps driven by IC engines [7-12]. Gasoline and other hydrocarbon fuels have very high energy densities, and would be the ideal fuel choice for free piston hydraulic pumps from an energy density standpoint. A breakthrough in the development of a reliable IC free piston engine hasn't occurred however, primarily resulting from several technical challenges including maintaining a constant compression ratio with the absence of a crank shaft, properly timing the ignition, and starting the engine. These challenges arise from the need to compress the air-fuel mixture in IC engines and to ignite the mixture at a certain compression ratio. Since monopropellants systems do not require compression, these problems are eliminated.

## 2. Description of Free Piston Hydraulic Pump

The basic power source design, illustrated in Figure 1, consists of two *Hot Gas Cylinders* and a *Hydraulic Cylinder*.

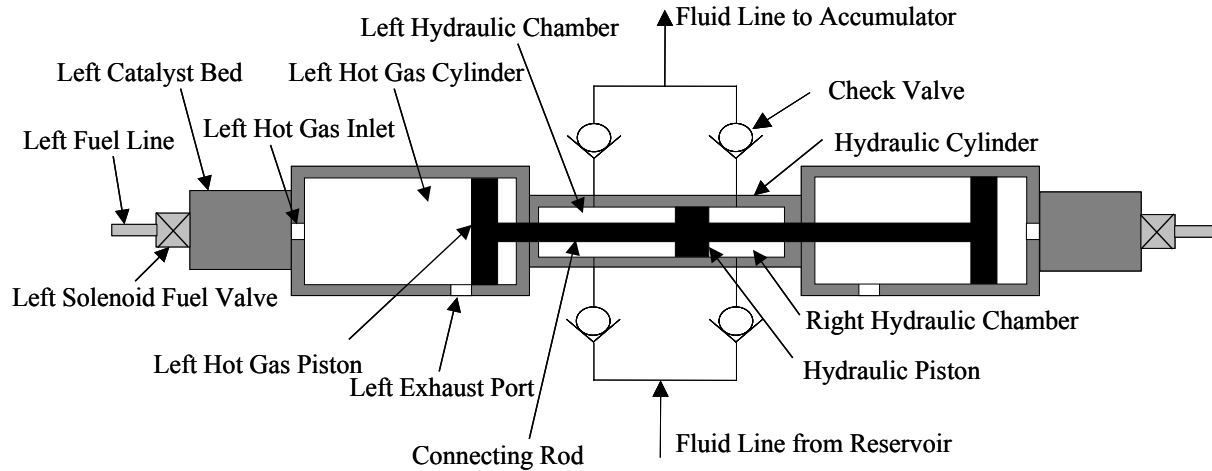
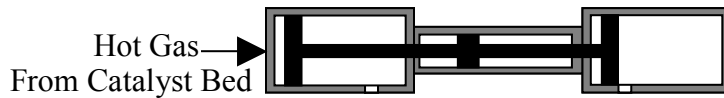


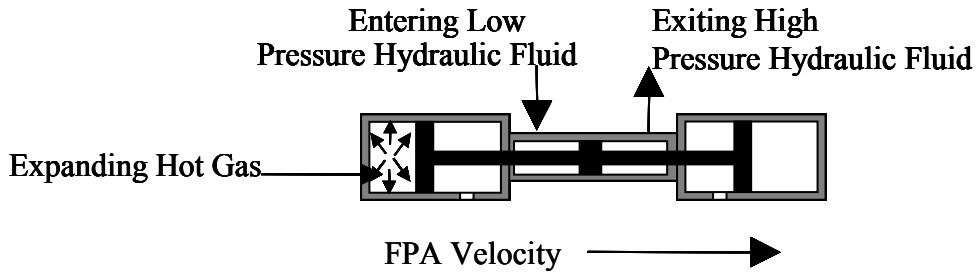
**Figure 1. Monopropellant Powered Free Piston Hydraulic Pump**

A cycle of the FPHP operation begins with the opening of the *Left Solenoid Fuel Valve*, allowing liquid monopropellant to flow into the *Left Catalyst Bed*. The *Catalyst Bed*, typically a metallic mesh, decomposes the liquid fuel into high pressure decomposition gases, which enter the *Left Hot Gas Cylinder* through the *Left Hot Gas Inlet* (Figure 2a). The expanding hot gas performs work on the *Left Hot Gas Piston*, forcing it to the right. Since the *Hot Gas Pistons* are rigidly connected to the *Hydraulic Piston* by a *Connecting Rod*, forming a single free piston assembly (FPA), the *Hydraulic Piston* is also forced to the right. This motion drives the hydraulic fluid in the *Right Hydraulic Chamber* through a *Check Valve* and into an accumulator, and draws low pressure hydraulic fluid from a reservoir into the *Left Hydraulic Chamber* (Figure 2b). When the piston reaches the end of its stroke, the gases are vented to the atmosphere through the *Left Exhaust Port*, which is machined into the cylinder (Figure 2c). This marks the end of the first stroke of one cycle. During the second stroke, fuel is injected into the *Right Catalyst Bed*, resulting in hot gas expansion in the *Right Hot Gas Cylinder*, which drives the piston to the left. This forces the hydraulic fluid in the *Left Hydraulic Chamber* into the high pressure

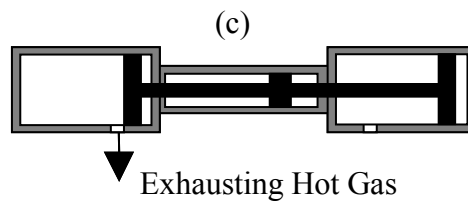
accumulator, and draws in more low pressure fluid into the *Right Hydraulic Chamber*. This cycle is then repeated. Thus, the FPHP is able to produce power with each stroke, since the *Check Valves* ensure that the hydraulic fluid is drawn into each *Hydraulic Chamber* when the piston moves in one direction, and pumped out at high pressure when the piston returns in the other direction. Since the area of the hydraulic piston is smaller than the hot gas piston, a pressure amplification is produced. This allows the FPHP to achieve higher pressures in the hydraulic fluid.



(a) Hot gas injected into cylinder



(b) Hot gas expands forcing FPA to the right



(d) Hot gas vents through exhaust port

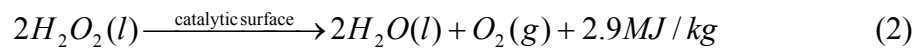
### Figure 2. Operation of Free Piston Hydraulic Pump

The design of this engine is much simpler than existing IC engines. There are no cams, complex exhaust port routing, or fuel mixture requirements. There is only one basic moving part: the FPA. This simple design results in a very reliable, robust machine capable of a long service life. Another important feature of this system is that as result of the simple radial geometry it can be manufactured fairly inexpensively.

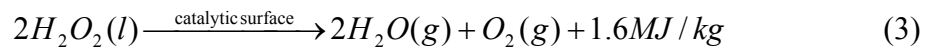
### 3. Hydrogen Peroxide as a Monopropellant

Although the free piston hydraulic pump outlined above could make use of any monopropellant fuel, hydrogen peroxide was chosen as the fuel of choice for the prototype. Hydrazine, the most widespread monopropellant in the aerospace community because of its high energy density of roughly 3.5 MJ/kg, is carcinogenic and very costly to handle. Hydrogen peroxide, on the other hand, has several characteristics making it much safer to use. First, it has a very low vapor pressure allowing personnel to handle the fuel without respirator systems. Furthermore, by diluting high strength peroxide with water, any immediate dangers can be easily eliminated. Finally, the decomposition products of hydrogen peroxide are hot steam and oxygen, which are nontoxic to humans. In addition to these benefits, since there is a relatively large market for high concentration hydrogen peroxide in the textile and integrated circuit industries, there is an infrastructure in place to commercially obtain the fuel. These advantages make hydrogen peroxide the best choice to study the monopropellant driven hydraulic pump in a laboratory environment.

One hundred percent hydrogen peroxide reacts according to the following reaction:



One disadvantage of hydrogen peroxide as a fuel is that the vaporization of the water produced from the reaction requires a large portion of the decomposition energy. Taking the vaporization of the water into account, the reaction can be expressed as:



This lower heating value (LHV) of the fuel of 1.6 MJ/kg, which takes into account energy lost to the latent energy of vaporization, is a more accurate representation of the total sensible energy available for mechanical work. Although pure hydrogen peroxide is ideal from an energy density standpoint, 70% and 90% hydrogen peroxide are far more

inexpensive and readily available for testing. The following table outlines the fuel energy densities, lower heating values, and decomposition temperatures for various concentrations of hydrogen peroxide:

Concentration	Fuel Energy Density	Lower Heating Value	Decomposition Temperature
100%	2.9 MJ/kg	1.6 MJ/kg	1269 K (1824 °F)
90%	2.6 MJ/kg	1.2 MJ/kg	1013 K (1364 °F)
70%	2.0 MJ/kg	0.4 MJ/kg	506 K (452 °F)

**Table 1. Comparison of Various Hydrogen Peroxide Concentrations**

These available sensible energy densities, or lower heating values, of the fuels are used to calculate efficiency of the FPHP:

$$\varepsilon = \frac{\text{hydraulic work extracted}}{\text{available sensible energy of fuel injected}} = \frac{P_{fH} V_{fH}}{LVH \cdot m_{fuel}} \quad (4)$$

where  $P_{fH}$  is the pressure of the hydraulic fluid,  $V_{fH}$  is the volume of hydraulic fluid pumped, and  $m_{fuel}$  is the mass of monopropellant fuel used. The use of the lower heating value, instead of the fuel energy density of the hydrogen peroxide, to calculate efficiencies gives a better indication of performance of the FPHP independent of the fuel used. Other propellants, like hydrazine, would not produce water as a product of decomposition, and would therefore not lose reaction energy to the vaporization of water.

## 4. Dynamic Analysis of Free Piston Hydraulic Pump

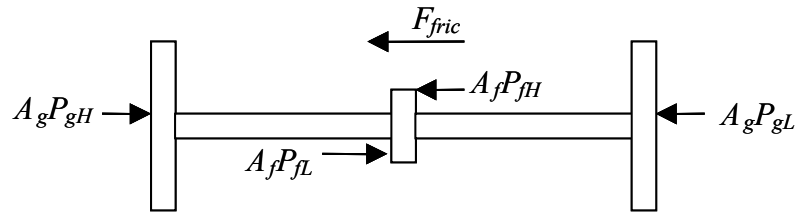
A dynamic analysis of the operation of the FPHP provides valuable insight into how to properly design and control the system.

### 4.1. Theoretical Modeling

The dynamics of the monopropellant driven FPHP are determined by the dynamics of the free piston assembly motion which are governed by:

$$\sum F = m\ddot{x} \quad (5)$$

where  $m$  denotes the mass of the FPA,  $\ddot{x}$  is its linear acceleration and  $\sum F$  is the sum of the forces acting on the FPA, which are illustrated in Figure 3.



$F_{fric}$  – Friction Force

$A_g$  – Area of Hot Gas Piston

$A_f$  – Area of Hydraulic Fluid Piston

$P_{gH}$  – Hot Gas Pressure on High Pressure Side

$P_{gL}$  – Hot Gas Pressure on Low Pressure Side

$P_{fH}$  – Hydraulic Fluid Pressure on High Pressure Side

$P_{fL}$  – Hydraulic Fluid Pressure on Low Pressure Side

**Figure 3. Free Body Diagram of Free Piston Assembly**

Inserting the individual force terms into Equation 5 yields:

$$m\ddot{x} = A_g (P_{gH} - P_{gL}) - A_f (P_{fH} - P_{fL}) - F_{fric} \quad (6)$$

Since the pressure of expanding hot decomposition gases,  $P_{gH}$ , provides the pumping force in the FPHP, the accurate modeling of this pressure is vital to analysis of the FPHP. The dynamics of the high-pressure hot gas cylinder are modeled assuming the hot gas enters the hot gas cylinder at the adiabatic decomposition temperature ( $T_{ad}$ ). The process is also assumed to be adiabatic since the duration of the stroke is not long enough for significant heat loss to occur. The pressure change is thus governed by:

$$\dot{P}_{gH} = \frac{1}{x} \left( \frac{\dot{m}_{gas} k R T_{ad}}{A_g} - k P_{gH} \dot{x} \right) \quad (7)$$

where  $R$  is the gas constant (ratio of universal gas constant to average molar mass),  $k$  is the specific heat ratio, and  $\dot{m}_{gas}$  is the mass flow rate of hot gas entering the hot gas cylinder. A more detailed derivation of Equation 7 is contained in Appendix A. Since no detailed analyses of hydrogen peroxide decomposition were found, it is assumed that the reaction dynamics for the hydrogen peroxide decomposition act as a pure time delay. Thus, the mass flow rate of hot gas into the hot gas cylinder equals the mass flow of fuel through the solenoid fuel valve,  $\dot{m}_{fuel}$ , shifted by a delay time,  $\tau$ , as illustrated in Figure 4. Equation 7 assumes that the volume of the hot gas cylinder is equal to zero when the FPA position,  $x$ , is equal to zero. Since the volume of the hot gas cylinder is not zero when the FPHP begins a stroke,  $x$  can be defined as:

$$x = x_n + x_{clearance} \quad (8)$$

where  $x_n$  is the FPA position, which is equal to zero at the beginning of a stroke, and  $x_{clearance}$ , is the effective clearance length in the hot gas cylinder:

$$x_{clearance} = \frac{V_{clearance}}{A_g} \quad (9)$$

where  $V_{clearance}$  is the volume of the hot gas cylinder at the beginning of each stroke. This extra volume includes any internal volume in the catalyst bed.

$$\dot{P}_{gH}(t) = \frac{1}{x_n(t) + x_{clearance}} \left( \frac{\dot{m}_{fuel}(t - \tau) k R T_{ad}}{A_g} - k P_{gH}(t) \dot{x}_n(t) \right) \quad (10)$$

The dynamics of the mass flow of the fuel through the solenoid valve are estimated since there is no available data on specific valve dynamics other than the valve response time. The flow is modeled as a linear ramp to the steady state value over the valve response time as illustrated in Figure 4.

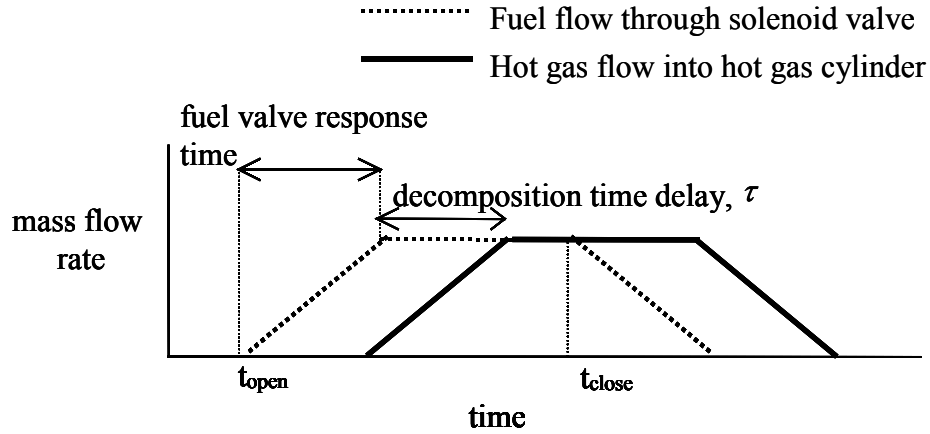


**Figure 4. Model of Fuel Flow Through Valve**

The steady state fuel flow is calculated from the valve flow equation as:

$$\dot{m}_{fuel,ss} = \rho C_v \sqrt{\frac{\Delta P}{\gamma}} \quad (11)$$

where  $\rho$  is the density of the fuel,  $C_v$  is geometry dependent valve constant,  $\Delta P$  is the pressure drop across the valve and  $\gamma$  is the specific gravity of the fuel (ratio of density of fuel to density of water).

Equation 10 is used to model the high pressure gas during the initial portion of the expansion stroke. Once the hot gas piston crosses the exhaust port, it is assumed that the exhaust ports are large enough to vent the high gas pressure to atmospheric pressure instantaneously.

As the gas in the high pressure hot gas cylinder expands, the gas in the low pressure hot gas cylinder is compressed. During the initial portion of this compression stage, while the exhaust port is still uncovered, the low pressure hot gas cylinder is still open to atmosphere so its pressure is assumed to be equal to atmospheric pressure. Once the low pressure hot gas piston passes the exhaust port, the low pressure side behaves as an air spring. Assuming the process is adiabatic, the pressure of the low pressure side is found from:

$$P_{gL}V^k = C \quad (12)$$

where  $V$  is the volume of the chamber,  $k$  is the specific heat ratio, and  $C$  is a constant determined from the pressure and volume when the low pressure hot gas piston crosses the exhaust port. Since the pressure drops across the hydraulic check valves are small compared to the changes in gas pressures and the high pressure hydraulic force,  $P_{fL}$  and  $P_{fH}$  are assumed to be constant with  $P_{fL}$  set to the hydraulic reservoir pressure and  $P_{fH}$  equal to the pumping pressure of the fluid in the accumulator. Since there are no side loads on the FPA, the friction is not dependent on the location of the FPA, as with a piston connected to a crankshaft, so  $F_{fric}$  is modeled as a constant.

## 4.2. Simulation Results

The first FPHP prototype was designed for a target power production of 3hp (2237 W) at an operating frequency ( $f$ ) of 10 Hz. The power output ( $P$ ) of the FPHP is calculated from:

$$P = 2P_{fH}A_fL_{stroke}f \quad (13)$$

where  $P_{fH}$  is the hydraulic pressure,  $A_f$  is the area of the hydraulic piston, and  $L_{stroke}$  is the stroke length of the FPA.

Initial design simulations were performed, assuming 90% hydrogen peroxide and properties for off the shelf fuel valves and catalyst beds, in order to determine a FPHP geometry that would provide the desired hydraulic power production of 3 hp at 1000 psig. In order to maximize efficiency, the simulation varied the fuel injection time to find the minimum amount of injected fuel that would result in a successful stroke. The efficiency ( $\varepsilon$ ) of the FPHP was then calculated as the ratio of work per stroke to the energy of the fuel injected (assuming a lower heating value (LHV) of 1.3MJ/kg for 90% hydrogen peroxide, which accounts for energy loss from vaporization of water):

$$\varepsilon = \frac{\text{work extracted per stroke}}{\text{energy of fuel injected per stroke}} = \frac{P_{fH} A_f L_{stroke}}{m_{fuel} LHV} \quad (14)$$

The simulation parameters, which represent the fuel properties, valve characteristics, and FPHP geometry of the target prototype, are listed in the Table 2.

H <sub>2</sub> O <sub>2</sub> Concentration	90%
Gas Constant ( $R_{H2O2}$ )	376 J/kgK
Specific Heat Ration ( $k$ )	1.27
Adiabatic Decomposition Temperature ( $T_{ad}$ )	1013 K
Steady State Fuel Mass Flow ( $\dot{m}_{fuel,ss}$ )	0.025 kg/sec
Decomposition Time Delay ( $\tau$ )	0.037 sec
Hydraulic Pumping Pressure in Accumulator ( $P_{fH}$ )	1000 psig
Hydraulic Reservoir Pressure ( $P_{fL}$ )	40 psig
Dry Friction ( $F_{fric}$ )	44 N
FPA Mass	0.544 kg
Hot Gas Cylinder Diameter	0.0465 m (1.83 in)
Stroke Length	0.06 m (2.36 in)
Gas Cylinder to Hydraulic Cylinder Area Ratio ( $A_g/A_f$ )	6.5
Clearance Volume ( $V_{clearance}$ )	$7.05 \times 10^{-5} \text{ m}^3$ (4.3 in <sup>3</sup> )

**Table 2. Design Simulation Parameters**

The fuel properties were taken from published data on hydrogen peroxide [1]. The FPHP geometry, mass properties, hydraulic pumping pressure, and reservoir pressure were taken from the design parameters of the prototype FPHP [13]. The dry friction was estimated from the forces required to manually push the FPA while assembling the pump. The steady state fuel flow through the solenoid fuel valves was estimated from Equation 11 assuming a  $C_v$  value of 0.015 (gal/min/psi<sup>1/2</sup>) and fuel tank pressure of 500 psig. The hot gas cylinder dead volume was calculated from the FPHP prototype data as well as the catalyst bed volume, and the decomposition time delay was estimated from literature on past hydrogen peroxide experiments [6].

The simulation, assuming the parameters in Table 2, resulted in an estimated efficiency of 21% for the initial prototype with a fuel injection time of 19ms. The simulation results showing the FPA displacement and velocity and hot gas behavior over several cycles are shown in Figures 5 and 6. Investigating the time duration of each stroke, it can be seen that a FPHP with these parameters is able to execute a full cycle, consisting of a right and left stroke, in approximately 0.07 seconds. Thus, according to the simulation, the FPHP can achieve the 10 Hz operating frequency required to produce the desired 3 hp output.

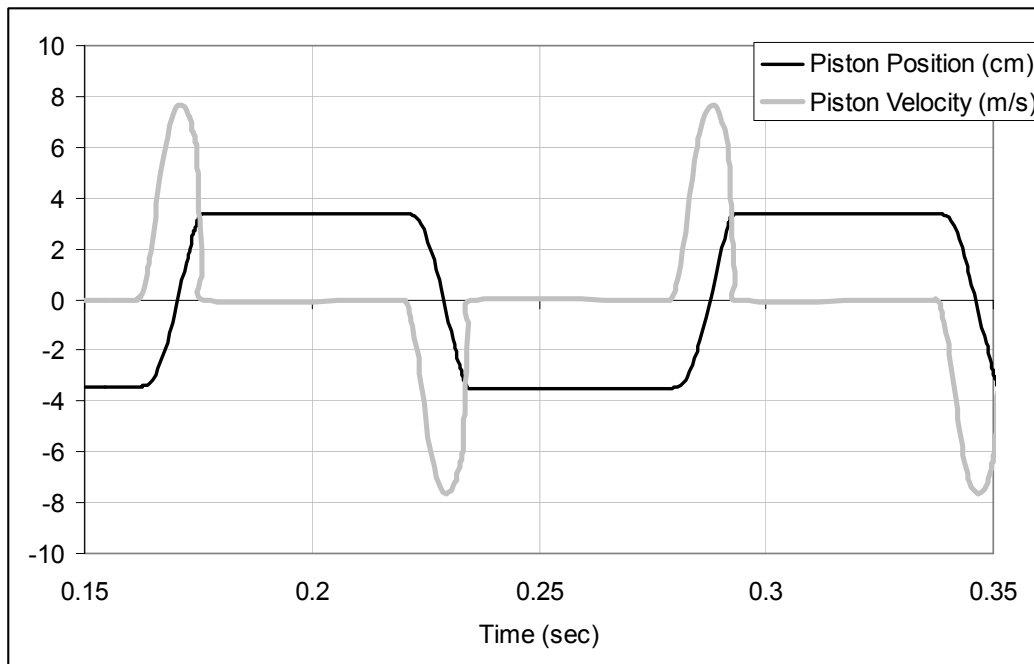


**Figure 5. Simulation Results for Free Piston Assembly Velocity and Position**

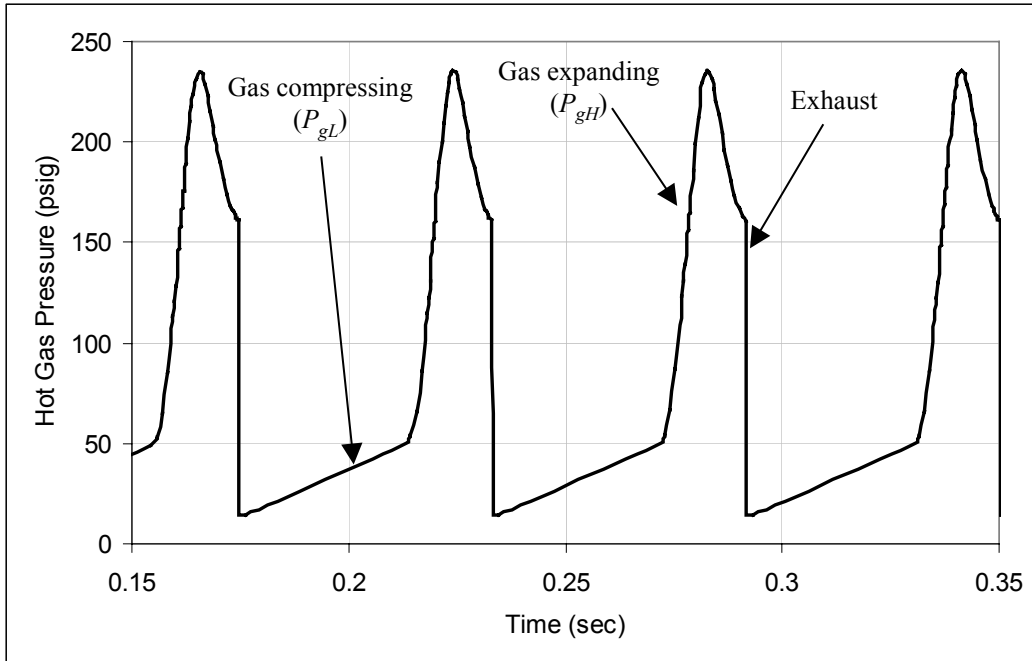


**Figure 6. Simulation Results for Hot Gas Pressure**

For the prototype design, the currently available catalyst beds and fuel valves limited how small we could make our hot gas cylinder dead volume and how high we could make the fuel flow rate. It is important to note that performance and efficiency could be improved by decreasing dead volume in the hot gas cylinder and by increasing the fuel flow rate with higher performance customized parts. Reducing the internal volume of the catalyst bed and thus reducing the dead volume connected to the hot gas cylinder can improve efficiency improved by reducing the amount of fuel required for each stroke. During the beginning of each stroke, the FPA is stationary until the pressure in the hot gas cylinder is high enough to overcome the force of the high pressure hydraulic fluid. Since the entire dead volume in the hot gas cylinder must be brought to this high pressure, a larger volume will require more hot gas particles and thus more fuel. Similarly, if the rate of injection of hot gas can be increased, higher initial pressures can be achieved, allowing more work to be extracted from the hot gas and increasing efficiency.

## 5. Experimental Free Piston Hydraulic Pump

In order to demonstrate the feasibility of the design and the accuracy of the simulation, a prototype FPHP, shown in Figure 7, was designed and constructed following the parameters listed in Table 2. Raade provides a comprehensive description of the design and manufacturing process for this design [11].

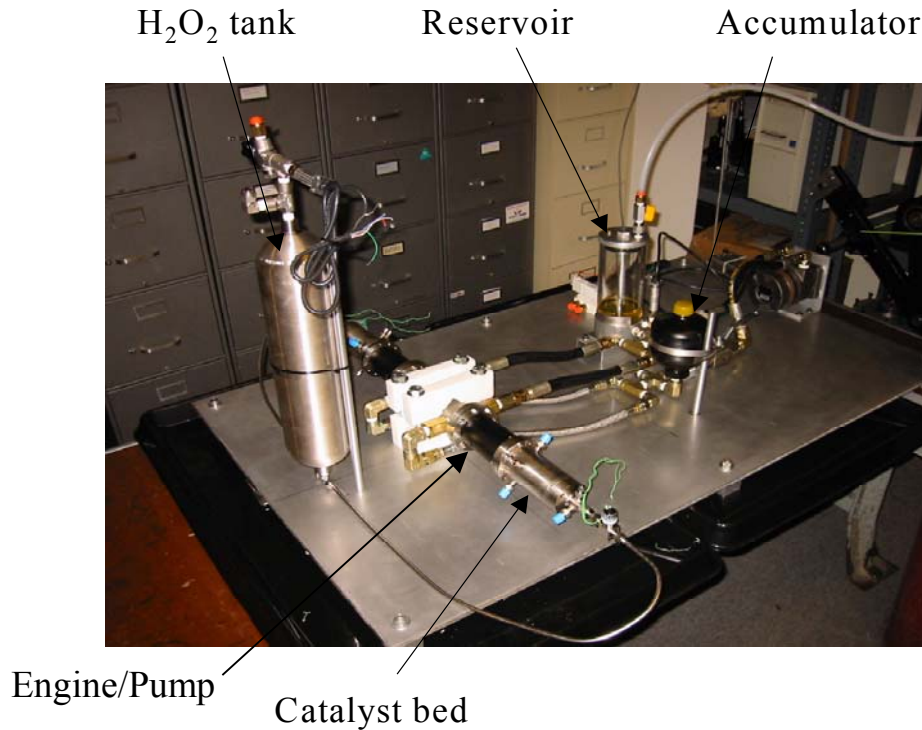


**Figure 7. Photo of the Experimental Power Source**

### 5.1. Hardware

The peripheral mechanical components of the FPHP system can be grouped into two main systems: the monopropellant fuel system and the hydraulic system. The fuel system layout is illustrated in Figure 8. The major components of this system are the fuel tank, fuel lines, solenoid fuel valves, and catalyst beds. The fuel tank must be pressurized in order to inject the fuel through the solenoid fuel valves and into the catalyst beds. For the experimental setup, compressed nitrogen at 500 psig, was used to pressurize the tank.

Future systems could use a secondary system to maintain tank pressure by decomposing a small portion of the monopropellant fuel. In order to increase the safety of the system a burst disk and emergency fuel dump valve were added to the system. A more detailed description of the safety measures taken for the system is contained in Appendix B.

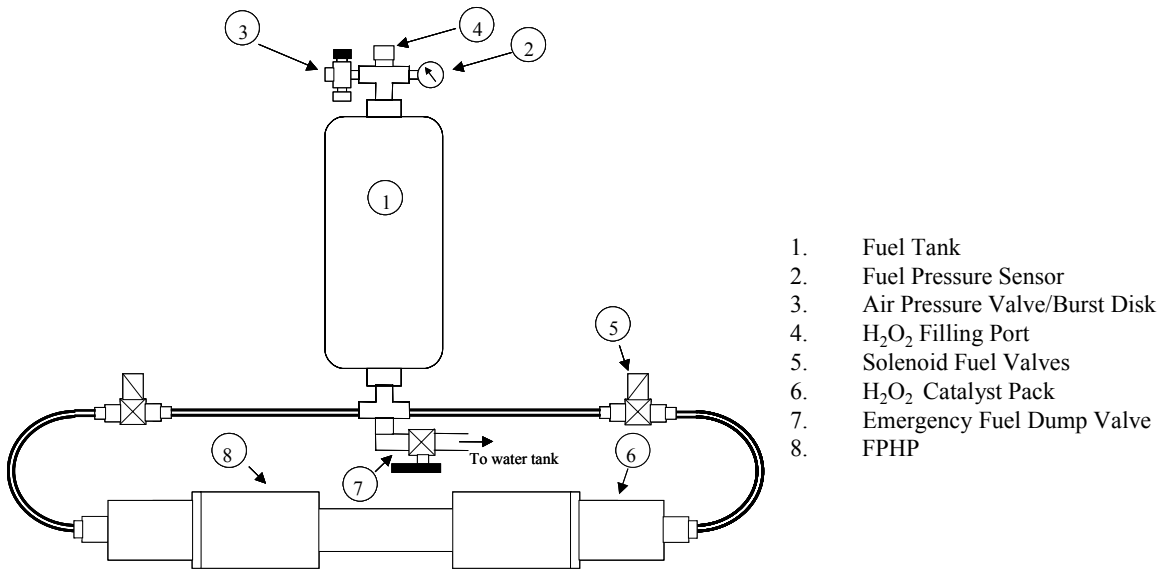


**Figure 8. Schematic of Monopropellant Fuel System**

The layout of the hydraulic system is illustrated in Figure 9. The FPHP is connected to the hydraulic system by four one-way check valves, which ensure that hydraulic fluid is properly routed from the hydraulic reservoir into the FPHP and from the FPHP into the high pressure accumulator. One unique property of this hydraulic system as compared to many traditional hydraulic systems is that the hydraulic reservoir is pressurized to 40 psig. Since the high velocity of the FPA produces high rates of hydraulic flow, the required pressure drop across the check valve between the reservoir and FPHP to produce this flow is higher than atmospheric pressure. Thus, if the reservoir were not pressurized, cavitation would occur, resulting in the formation of bubbles in the hydraulic fluid. In order to complete the hydraulic circuit, a hydraulic motor was added to the system between the high pressure accumulator and the low pressure reservoir. A pressure relief valve was also added to the system, in parallel to the motor. This spring loaded check valve was set to open at approximately 1000 psig to allow fluid to bypass

the motor and flow directly from the accumulator to the reservoir if the accumulator pressure became too great. This check valve also allowed the simulation of a constant 1000 psig load on the FPHP. By closing a shutoff valve to the motor, hydraulic fluid could be forced to flow through the relief valve while maintaining a pressure near 1000 psig in the accumulator. The 1000 psig backpressure seen by the FPHP in this case is virtually identical to what the pump would experience with a 1000 psig load on the motor.

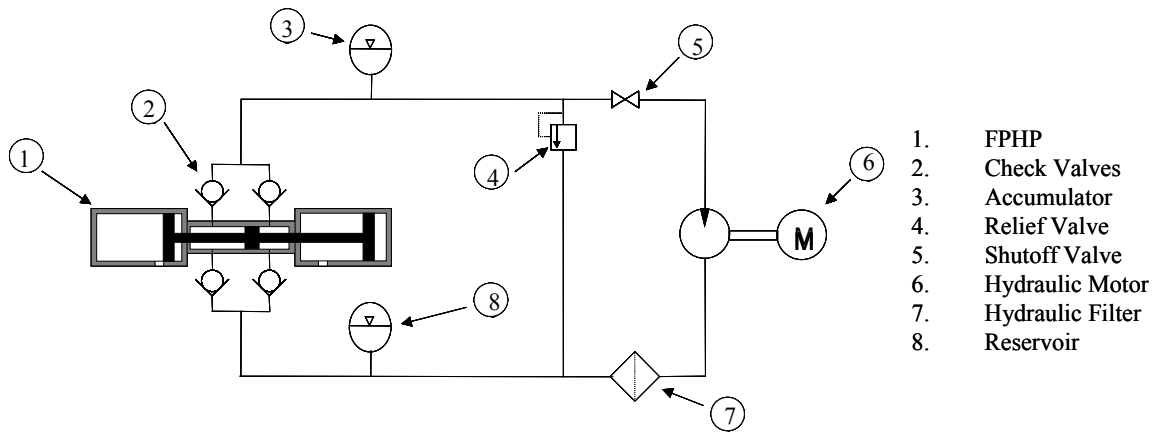


**Figure 9. Hydraulic System for Free Piston Hydraulic Power Source**

## 5.2. Experimental Results

The experimental FPHP was tested using 90% hydrogen peroxide fuel with the shutoff valve to the hydraulic motor closed to simulated a 1000 psig load as described above. Figure 10 shows the recorded hydraulic accumulator pressure for a test that was performed while manually pulsing the solenoid fuel valves. Once the FPHP was successfully tested in this manual mode, it was tested using a computer to control the time each solenoid fuel valve was open. Opening one fuel valve for 500 ms and then waiting 5000 ms before pulsing the opposite valve achieved the best results. Figure 11 illustrates the recorded hot gas pressures in both hot gas cylinders over several cycles. Figure 12 shows a more detailed view of the hot gas pressures during one stroke of the FPHP. Even though the FPHP successfully pumped hydraulic fluid, several undesirable

phenomenons were observed during testing. First, the FPA exhibited stiction-like behavior, with many of the strokes consisting of a series of small jerky motions instead of one smooth, continuous stroke. Second, most of the strokes resulted in a very slow exhaust of the hot gas, which was observed by a hissing sound. This contrasted with the much louder bursts and rapid exhaust observed during past tests when 150 psig nitrogen gas was used to drive the FPA for leak testing of the hydraulic system. Third, over the several cycles, the gas pressures on both sides of the FPHP gradually built up. Eventually, the excessive pressure on both sides prevented the FPHP from pumping at all, and the FPA remained stationary.

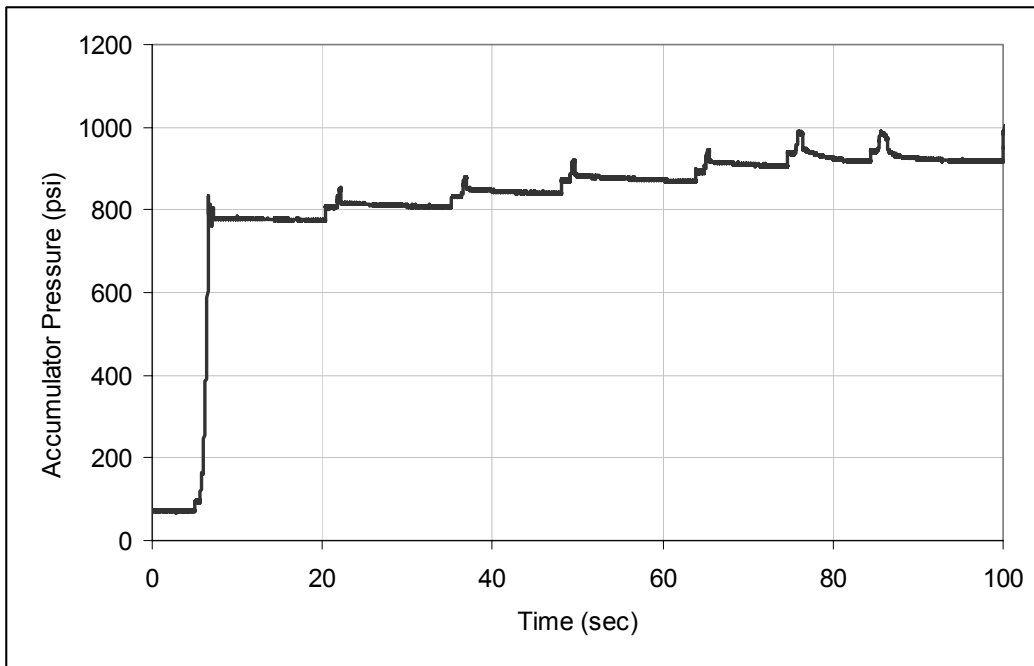


**Figure 10. Experimental Accumulator Pressure with Manual Fuel Valve Pulse**

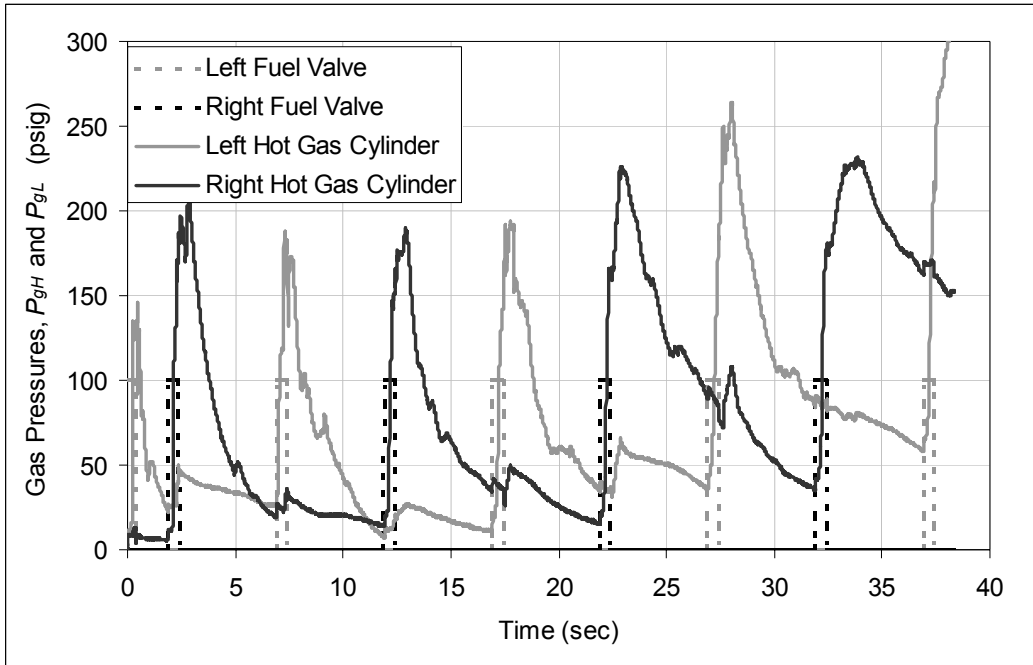


**Figure 11. Experimental Hot Gas Pressure with 500ms Injection Time**

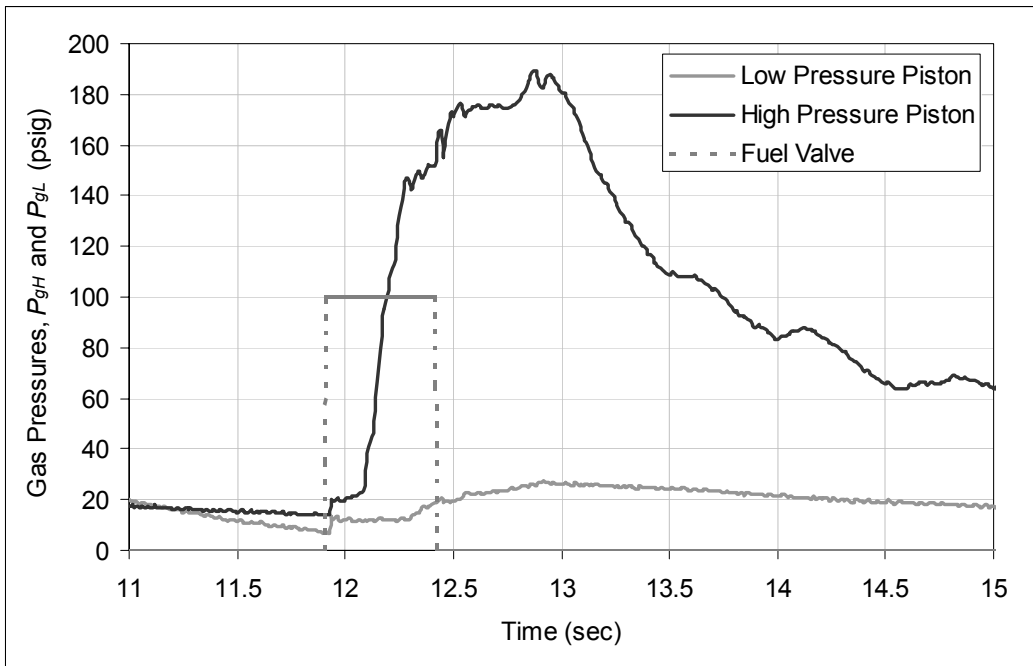


**Figure 12. Experimental Hot Gas Pressure Over Single Stroke**

## 6. Discussion

Although the experimental FPHP successfully pumped hydraulic fluid at pressures near 1000 psig, the experimental results differed greatly from the simulation results. During the simulation, short injection times of 19 ms produced quick pulses on the order of tens of milliseconds as shown in Figure 6, while much larger injection times of 500 ms were required on the actual system, producing much more gradual pressure rises and strokes lasting on the order of seconds as shown in Figure 11. Upon careful evaluation of the experimental results and the prototype hardware this discrepancy may be the result of poor delivery of the monopropellant from the fuel valve to the catalyst bed. Since off-the-shelf fuel valves and catalyst beds were used, the required fittings to connect the valve and catalyst bed were rather large, creating a large amount of dead space between the solenoid fuel valve and catalyst bed. Figure 13 shows an enlarged view of the interface between the solenoid fuel valve and the catalyst bed. In this picture, it can be seen that there is approximately three inches of  $\frac{1}{4}$ " tubing between the body of the fuel valve and the weld on the catalyst bed casing which indicates the beginning of the silver catalyst mesh. The sensor ports on the base of the catalyst bed, which can be more clearly seen in the supplemental photos in Appendix C, also add extra volume between the fuel valve and catalyst bed. The diagram in Figure 14 further illustrates the interface between the fuel valve and the catalyst bed.

Taking the volume between the fuel valve and the catalyst bed into consideration, the slow pressure rise and long injection times required for the experimental system appear to be the result of a large portion of the injected fuel collecting in this empty volume instead of entering the catalyst bed and decomposing. Thus it is hypothesized that the actual flow rate of hot gas into the cylinder is much lower than the mass flow rate of monopropellant from the fuel valve.

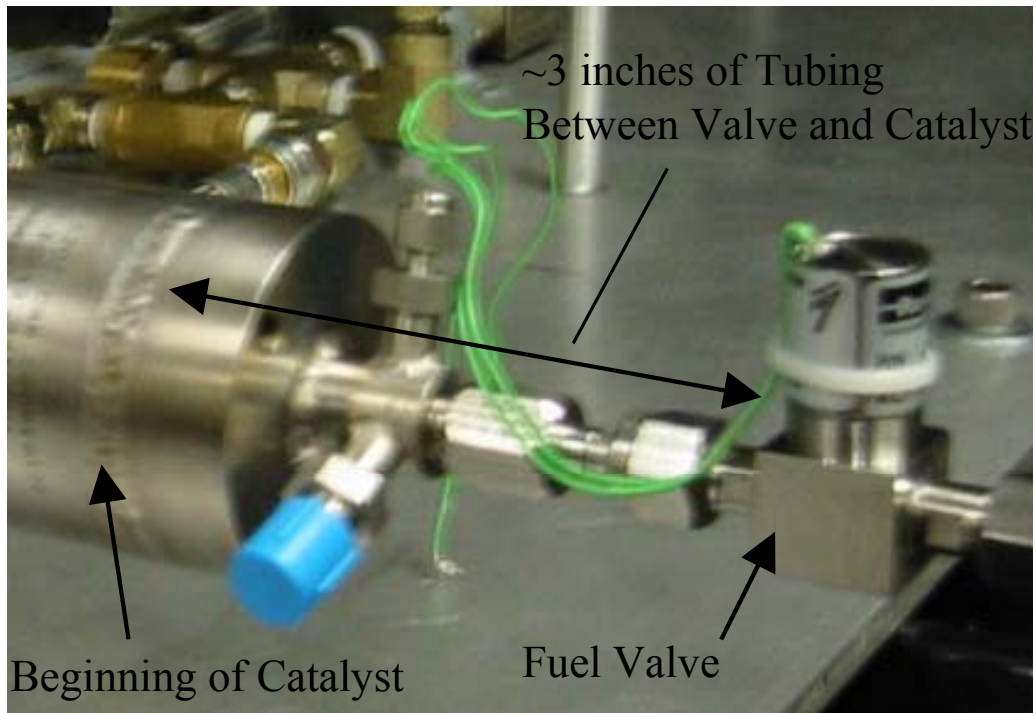


**Figure 13. Photo of Interface Between Fuel Valve and Catalyst**

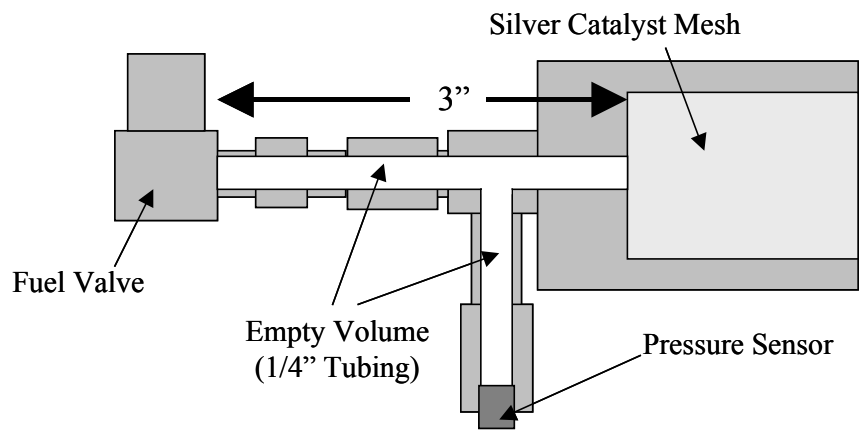


**Figure 14. Diagram of Interface Between Fuel Valve and Catalyst**

In order to verify this hypothesis, several modifications were made to the original simulation. First, the hydraulic pumping pressure was changed from 1000 psig to 900 psig since Figure 10 shows that the hydraulic relief valve is set closer to this value. Second, the dead volume in the hot gas cylinder was increased from  $7.05 \times 10^{-5} \text{ m}^3$  (4.3 in<sup>3</sup>) to  $1.15 \times 10^{-4} \text{ m}^3$  (7.0 in<sup>3</sup>) to account for the extra dead volume between the fuel valve and the catalyst bed not accounted for in the initial design. Finally, the steady state mass flow rate was changed from 0.025 kg/sec to 0.001 kg/sec to account for the hypothesis that the injected fuel collects in the space between the valve and catalyst, entering the catalyst at a much lower rate. The results of the modified simulation, plotted against the experimental data in Figure 15, support the hypothesis that the monopropellant is in fact pooling between the valve and catalyst.

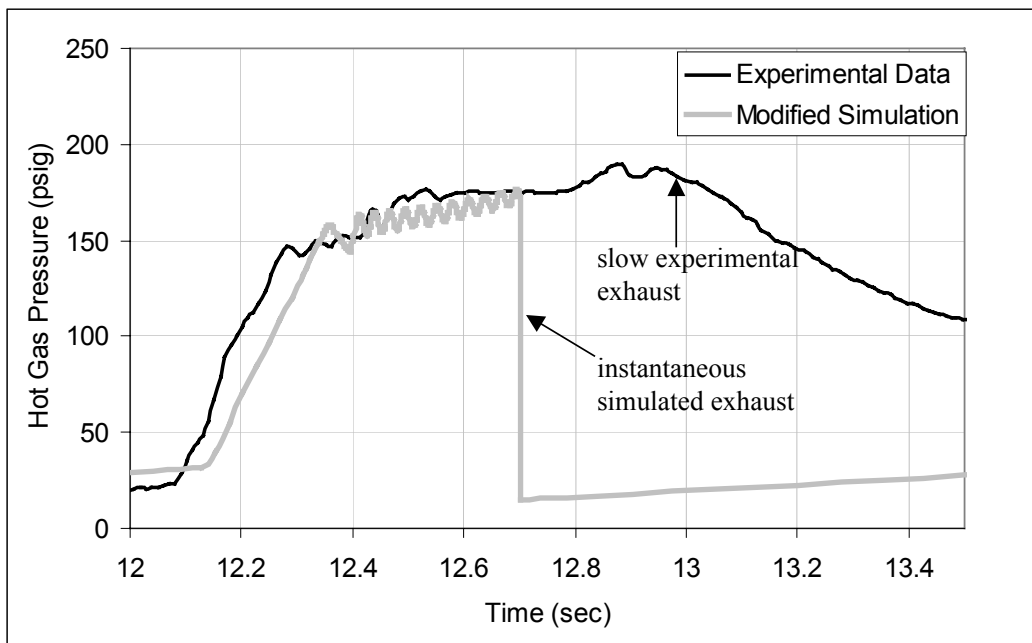


**Figure 15. Comparison of Experimental Data with Modified Simulation**

One important characteristic of both the experimental and simulated results in Figure 15 is the smooth initial rise in pressure followed by oscillations in the pressure. This rise in pressure corresponds to the stage in the stroke when the FPA is stationary since the hot gas pressure is not high enough to overcome the high hydraulic force on the hydraulic

piston. Looking at Equation 8, which governs the hot gas pressure dynamics, the FPA velocity term,  $\dot{x}$ , is initially zero. Thus, the pressure change is positive since the term governed by the fuel injected,  $\dot{m}_{fuel}$ , is always positive. Once the FPA begins to move, the velocity is no longer zero, and the negative FPA velocity term eventually dominates the positive fuel injection term since the actual rate of fuel entering the catalyst bed is so small. This causes the time derivative of the pressure to become negative. As the hot gas pressure drops, the hydraulic pressure slows the FPA. When the FPA is significantly slowed or sometimes stopped entirely, the positive fuel injection term of Equation 8 again dominates, causing the time derivative of the pressure to become positive. As the hot gas pressure increases, it causes the FPA velocity to increase, resulting in a new drop in the hot gas pressure. This cycling of this process results in the pressure oscillations. These oscillations also account for the stiction-like behavior of the FPA, which was observed during testing as the pressure oscillations caused FPA velocity to cyclically increase and then drop to zero.

One difference that remains between the modified simulation and the experimental result is the venting rate of the hot gas at the end of the stroke. The simulation assumes that the exhaust port is fully uncovered and the hot gas drops sharply at the end of the stroke. The hot gas in the experimental test vented much slower, as illustrated by the shallow negative slope after 13 seconds of the experimental curve in Figure 15. This poor venting results from the slow velocity at the end of each stroke since the FPA doesn't have enough momentum to fully uncover the exhaust ports.

The collection of fuel between the valve and catalyst bed also accounts for the occasional sharp increases in gas pressure long after the fuel valves have been closed. A good example of this is the rise in pressure in the right gas chamber in Figure 12 at 14.2 seconds. This pooling of fuel also creates a steady generation of hot gas on both sides of the FPHP as the collected fuel slowly drains into both catalyst beds. This gradual gas generation, along with the slow venting rates, accounts for the gradual pressure rise in both hot gas cylinders as seen in Figure 11, which eventually prevented the FPA from moving.

## **7. Conclusions**

The simulation and experimental results of a novel monopropellant driven free piston hydraulic pump have been presented. The simple and compact design of the FPHP allows inexpensive and robust power supply systems to be created. These systems, which offer improved energy and power density over electrical systems and the ability to produce intermittent power without idling in oxygen free environments could have applications in a variety of mobile robotics applications. Although the experimental prototype of the monopropellant driven free piston hydraulic pump was not able to produce the target 3 hp power output, it did demonstrate the feasibility of using a monopropellant to drive a piston engine and pump hydraulic fluid. The analysis of the experimental results also revealed that an integration of the fuel valve and catalyst bed is essential to improve the delivery of the fuel to the catalyst bed. This knowledge can be applied to future versions of this type of system to greatly improve performance and make field versions of monopropellant driven free piston hydraulic pumps a reality.

## 8. References

1. McCormick, J.C. "Hydrogen Peroxide Rocket Manual", FMC Corporation, 1967.
2. Stokes, P.R. "Hydrogen Peroxide for Power and Propulsion", presented at the London Science Museum, 1998.
3. Dismukes, Kim (curator). "Auxiliary Power Units", NASA Human Spaceflight Website. [spaceflight.nasa.gov/shuttle/reference/shutref/orbiter/apu/](http://spaceflight.nasa.gov/shuttle/reference/shutref/orbiter/apu/)
4. Johnsen, E.G. and Corliss, and W.R. "Teleoperator and Human Augmentation", AEC-NASA Technology Survey, NASA Document SP-5047, 1967.
5. Amendola, S.C. and Petillo, P.J. "Engine Cycle and Fuels for Same", United States Patent # 6,250,078 B1, 2001.
6. Barth, E.J., Gogola, M.A., Wehrmeyer, J.A., and Goldfarb, M. "The Design and Modeling of a Liquid-Propellant-Powered Actuator for Energetically Autonomous Robots". 2002 ASME International Mechanical Engineering Congress and Exposition (IMECE).
7. Beachley, N.H. and Fronczak, F.J. "Design of a Free-Piston Engine Pump", SAE paper 921740, 1992.
8. Dalton, T.B. "Dual Pressure Hydraulic Pump", United States Patent # 3,985,470, 1976.
9. Heintz, R.P. "Free-Piston Engine-Pump Unit", United States Patent # 4,087,205, 1978.
10. Heintz, R.P. "Theory of Operation of a Free Piston Engine-Pump", SAE paper 859315, 1985.
11. Li, L.J. and Beachley, N.H. "Design Feasibility of a Free Piston Internal Combustion Engine/Hydraulic Pump", SAE paper 880657, 1988.
12. Tikkanen, S. and Vilenius, M. "On the Dynamic Characteristics of the Hydraulic Free Piston Engine", Second Tampere International Conference on Machine Automation, 1998.
13. Raade, Justin W. "Design and Testing of a Monopropellant Powered Free Piston Hydraulic Pump", Masters Thesis University of California at Berkeley, 2003.

## 9. Appendix A. Derivation of Hot Gas Dynamics Equation

Starting with the first law of thermodynamics, the conservation of energy for any control volume is:

$$E_{in} - E_{out} = \Delta E_{system} \quad (\text{A-1})$$

By taking the time derivative of both sides of Equation A-1, one yields:

$$\dot{E}_{in} - \dot{E}_{out} = \Delta \dot{E}_{system} \quad (\text{A-2})$$

Assuming uniform fluid properties, the general form of Equation A-2 for a control volume can be expressed as:

$$\sum \dot{m}_i \left( h_i + \frac{v_i^2}{2} + gz_i \right) - \sum \dot{m}_e \left( h_e + \frac{v_e^2}{2} + gz_e \right) + \dot{Q} - \dot{W} = \frac{d}{dt} E_{system} \quad (\text{A-3})$$

where  $\dot{m}_i$  and  $\dot{m}_e$  are the mass flow rates into and out of the system,  $h$  is specific enthalpy,  $v$  is velocity,  $g$  is gravity,  $z$  is height,  $\dot{Q}$  is the total rate of heat flow into the system, and  $\dot{W}$  is the rate of work done by the system on the surroundings.

The hot gas cylinder of the FPHP is modeled as a control volume with the hot oxygen and steam entering at the adiabatic decomposition temperature ( $T_{ad}$ ) of the hydrogen peroxide as illustrated in Figure A-1.

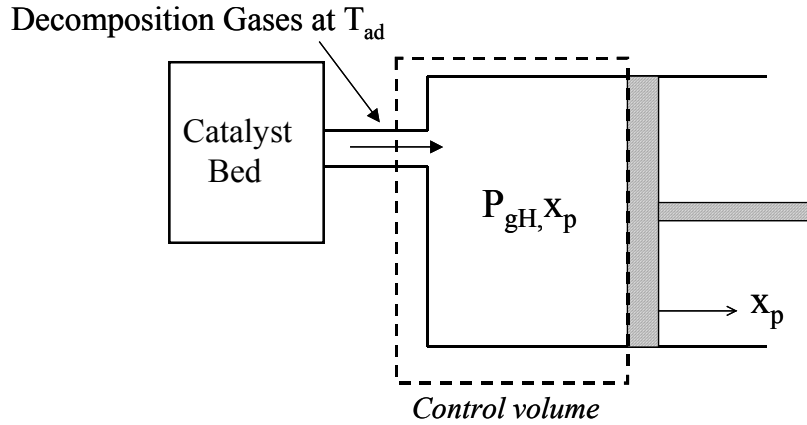


**Figure A-1. Control Volume for Hot Gas Cylinder**

Since each stroke occurs in a relatively short time, very little heat will be lost through the cylinder walls. It is therefore a reasonable assumption to assume the process is adiabatic, eliminating the  $\dot{Q}$  term. The kinetic and gravitational energy of the hot gas will be much smaller than the enthalpy so the  $v_i^2/2$  and  $gz_i$  terms can be eliminated. Thus, for the model of the hot gas cylinder, Equation A-3 can be simplified to:

$$\dot{m}_i h_i - \dot{W} = \frac{d}{dt} E_{system} \quad (A-4)$$

Now the rate of work that the system performs on the surroundings can be calculated from the FPA velocity,  $\dot{x}_p$ , the hot gas pressure,  $P_{gH}$ , and the hot gas piston area,  $A_p$ :

$$\dot{W} = A_p P_{gH} \dot{x}_p \quad (A-5)$$

The energy of the compressible gas system,  $E_{system}$ , is the sum of the internal energy,  $U$ , the kinetic energy,  $KE$ , and potential energy  $PE$ .

$$E_{system} = U + KE + PE \quad (A-6)$$

The kinetic and potential energy are negligible compared to the internal energy of the hot compressed gas. Thus  $KE$  and  $PE$  can be ignored:

$$E_{system} = U \quad (A-7)$$

The internal energy can be calculated from gas temperature in the hot gas cylinder,  $T_g$ , the mass of the gas,  $m_p$ , and the specific energy,  $c_v$  through an ideal gas approximation:

$$U = m_p c_v T_g \quad (A-8)$$

The mass can be also be expressed as the product of the density,  $\rho$ , hot gas piston area, and FPA displacement,  $x_p$ :

$$m_p = \rho A_p x_p \quad (A-9)$$

Assuming ideal gas properties, the specific heat can be calculated from the gas constant,  $R$  and the specific heat ratio  $k$ , which are known properties of the gas:

$$c_v = \frac{R}{k-1} \quad (A-10)$$

Inserting Equations A-9 and A-10 into Equation A-8 yields:

$$U = \frac{A_p x_p \rho R T_g}{k-1} = E_{system} \quad (A-11)$$

The ideal gas law can be written as:

$$P_{gH} = \rho R T_g \quad (A-12)$$

Substituting Equation A-12 into Equation A-11 yields:

$$E_{system} = \frac{A_p x_p P_{gH}}{k-1} \quad (A-13)$$

Differentiating Equation A-13 with respect to time:

$$\frac{d}{dt} E_{system} = \frac{A_p}{k-1} (\dot{x}_p P_{gH} + x_p \dot{P}_{gH}) \quad (A-14)$$

Since ideal gas properties are assumed, the enthalpy of the incoming hot gas,  $h_i$ , can be determined from the gases temperature, which is assumed to be the adiabatic decomposition temperature,  $T_{ad}$ :

$$h_i = c_p T = k c_v T = \frac{kR}{k-1} T_{ad} \quad (A-15)$$

Substituting Equations A-5, A-14, and A-15 into Equation A-4 yields:

$$\dot{P}_{gH} x_p + k P_{gH} \dot{x}_p = \dot{m}_i \frac{kRT_{ad}}{A_p} \quad (A-16)$$

Now if the reaction dynamics of the decomposition of liquid fuel to hot gas is modeled as a pure time delay,  $\tau$ , the mass flow of hot gas can be found from the flow of fuel into the catalyst bed as:

$$\dot{m}_i(t) = \dot{m}_{fuel}(t - \tau) \quad (A-17)$$

Combining Equations A-16 and A-17 and reordering terms produce the final equation for the hot gas dynamics:

$$\dot{P}_{gH}(t) = \frac{1}{x(t)} \left( \frac{\dot{m}_{fuel}(t - \tau) kRT_{ad}}{A_g} - k P_{gH}(t) \dot{x}(t) \right) \quad (A-18)$$

## **10. Appendix B. Safety Procedures for H<sub>2</sub>O<sub>2</sub> System Design and Handling**

Since high concentration hydrogen peroxide is an energetic compound, there are several key factors that were considered when designing the hydrogen peroxide system and handling the fuel. Below is an outline of safety procedures followed during experimentation with the monopropellant pump prototype. It should not be viewed as comprehensive however, and appropriate training in hydrogen peroxide use should always be sought before handling the fuel.

### **10.1. Materials and Passivation**

All of the wetted components in the fuel system are either 316 or 304 stainless steel, Viton, or Teflon which are all compatible with hydrogen peroxide for the time scales used in our testing. In addition, all of the stainless steel components were given a nitric acid passivation according to the ASTM A967 standard. This process is standard with hydrogen peroxide systems, and is performed in order to remove any oxides or residues on the hardware that could promote decomposition. While Teflon, and many other fluoro-polymers can be safely used for long-term storage of hydrogen peroxide, passivated 316 and 304 stainless steels are appropriate only for short term usage on the order of a few hours to a week depending on the quality of the material and passivation performed.

### **10.2. Pressure Relief and Fuel Dump Valve**

A pressure relief rupture disc has been incorporated into the fuel system as an added safety feature in the event of undesired decomposition and pressure buildup in the fuel tank. The rupture disc is a passive pressure relief device designed to rupture at 1900 psig, prior to failure of any other system components, allowing the pressurized gas to vent. Rupture discs were also installed on each of the hot gas cylinders to vent at 1000 psig in the case of a seized FPA. While the burst discs increase the safety level of the system, it is important to note that burst discs could be inadequate in the event of a major contamination of the hydrogen peroxide, and should never be viewed as a replacement of proper material selection and proper fuel handling procedures. In addition to the burst

disk, a fuel dump valve was added to the fuel tank. This valve allows the fuel in the tank to be quickly emptied into a bucket of water in the case of an emergency. By dumping the fuel into water, it can be diluted to a much lower concentration that will no longer produce high pressure gas.

### **10.3. Personal Safety Equipment**

When handling the hydrogen peroxide fuel, protective gear consisting of goggles, a supplemental full-face shield, a full vinyl apron with sleeves, rubber boots, and long neoprene gloves were always worn. This gear protects the user from physical contact with the hydrogen peroxide. A polycarbonate shield and several large barriers also surrounded the apparatus during operation as an additional safety measure. Running water, as well as an emergency eyewash and shower, were also readily available.

### **10.4. Training**

In order to become familiar with standard handling and operating procedures with hydrogen peroxide, the members of the lab attended a training session at General Kinetics, LLC. General Kinetics is a private company located in Lake Forest, California that specializes in the design of high concentration hydrogen peroxide systems and training for operation of such systems. This training included both classroom training and a safety test with the prototype pump using 90% peroxide to ensure system safety. FMC, the primary supplier of high concentration peroxide, also required an on site visit by a company representative to review the safety of the laboratory and to provide a safety training at the University facilities where the prototype was tested.

### **10.5. Disposal of H<sub>2</sub>O<sub>2</sub>**

Since only small quantities of high concentration peroxide were ordered, there was little or no hydrogen peroxide to dispose of after the test. The reaction of the hydrogen peroxide in the catalyst bed resulted in oxygen and steam, which are benign to the environment. Any extra hydrogen peroxide at the end of testing was decomposed using the catalyst beds to break it into steam and oxygen. Any small spills were diluted with water to levels below 3%, which is equivalent to the peroxide available at pharmacies and benign to the environment.

## **10.6. Emergency Situation Procedure**

Laboratory specific emergency procedures were in place and reviewed prior to any testing with the hydrogen peroxide. In the case of contact with hydrogen peroxide, the contacted area would be flushed with large amounts of water and medical attention would be sought immediately. Any spillage would be neutralized with water and disposed of properly.

## 11. Appendix C. Photographs of Experimental System

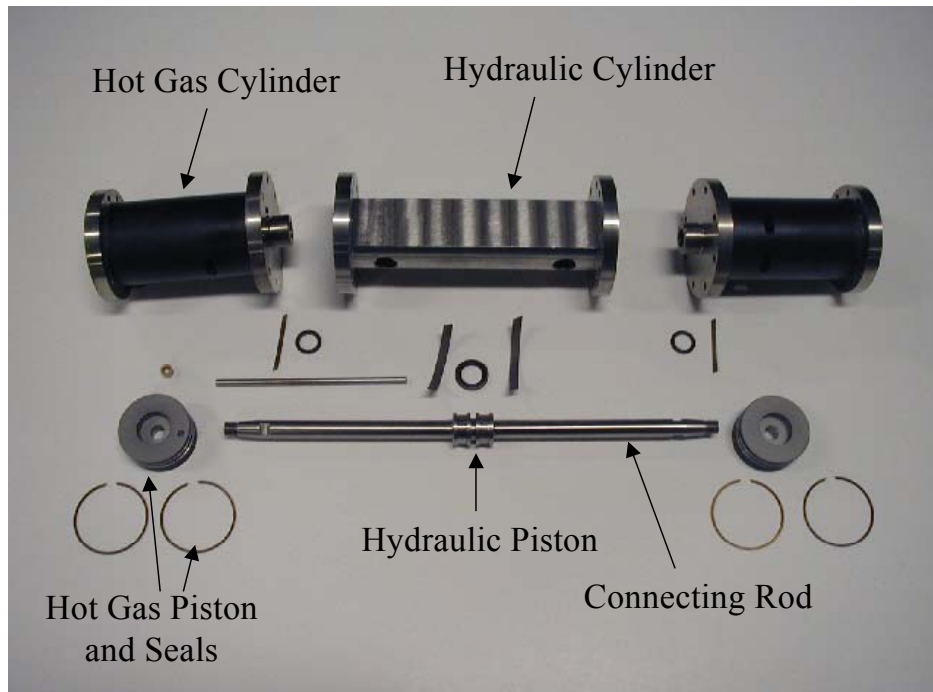


**Figure C-1. Disassembled FPHP**

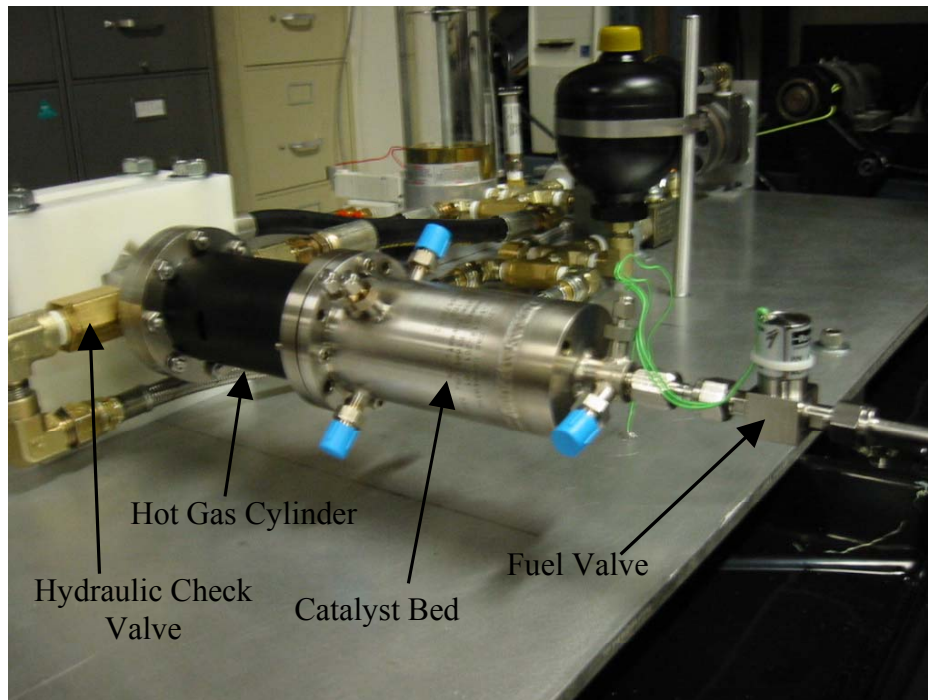


**Figure C-2. Close up of Fuel Valve – Catalyst Bed Assembly**

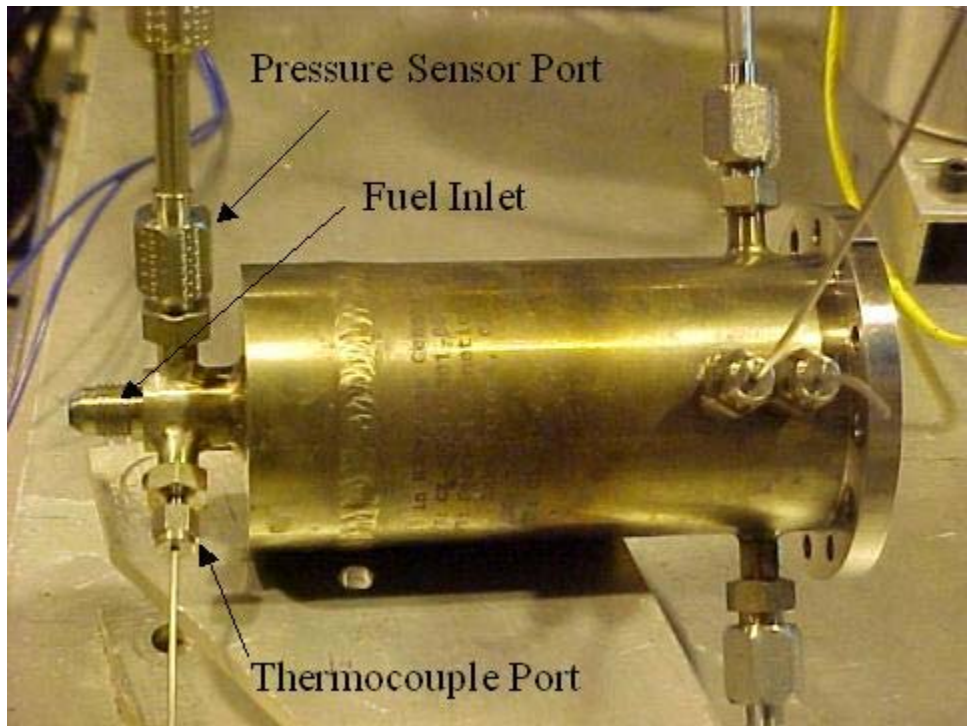


**Figure C-3. Catalyst Bed**



**Figure C-4. Safety Testing of System at General Kinetics' Facility**



**Figure C-5. Loading Hydrogen Peroxide Propellant**

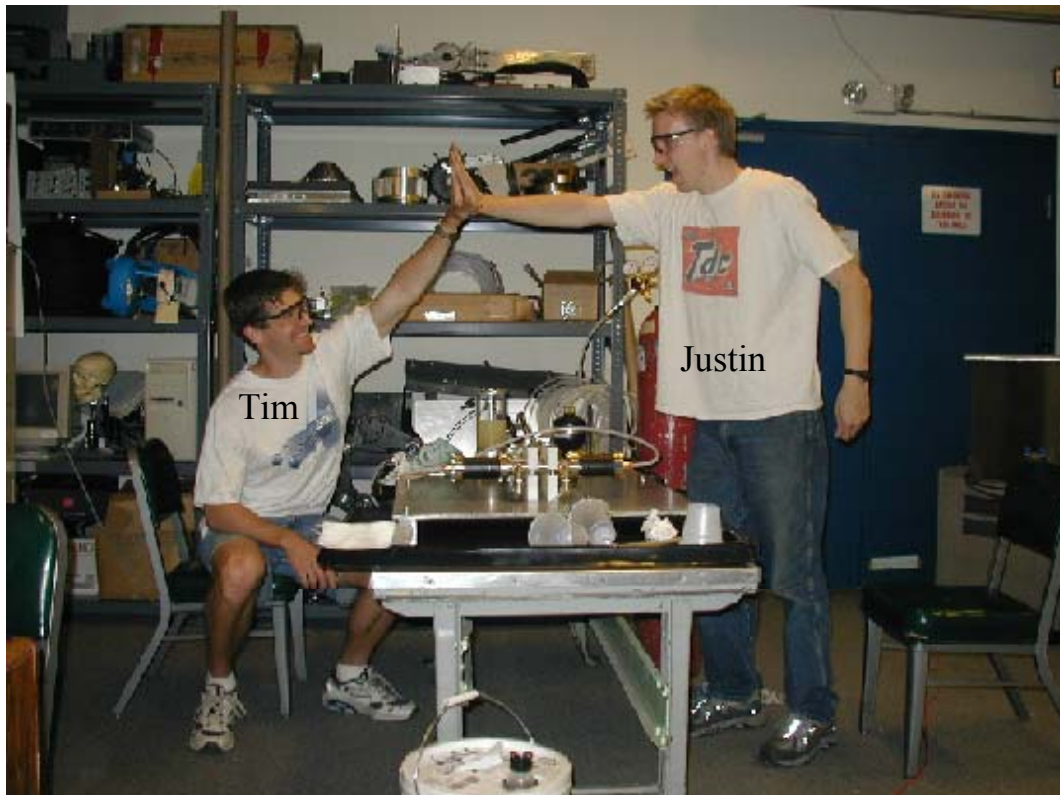


**Figure C-6. Successful Test of FPHP Using Compressed Air**